# Quarterly Progress Report

# N01-NS-1-2333

## *Restoration of Hand and Arm Function by Functional Neuromuscular Stimulation*

**Period covered: April 1, 2006 to June 30, 2006**


**Principal Investigator:** Robert F. Kirsch, Ph.D.

**Co-Investigators:**

Patrick E. Crago, Ph.D.
P. Hunter Peckham, Ph.D.
J. Thomas Mortimer, Ph.D.
Kevin L. Kilgore, Ph.D.
Michael W. Keith, M.D.
David L. Wilson, Ph.D.
Dawn Taylor, Ph.D.
Joseph M. Mansour, Ph.D.
Jeffrey L. Duerk, Ph.D.
Wyatt S. Newman, Ph.D.
Harry Hoyen, M.D.
John Chae, M.D.
Dustin Tyler, Ph.D.

**Program Manager:** William D. Memberg, M.S.

Case Western Reserve University
Wickenden 407
10900 Euclid Avenue
Cleveland, OH 44106-7207
216-368-3158 (voice)
216-368-4969 (FAX)
rfk3@po.cwru.edu

## Contract abstract

The overall goal of this contract is to provide virtually all individuals with a cervical level spinal cord injury, regardless of injury level and extent, with the opportunity to gain additional useful function through the use of FNS and complementary surgical techniques. Specifically, we will expand our applications to include individuals with high tetraplegia (C1-C4), low tetraplegia (C7), and incomplete injuries. We will also extend and enhance the performance provided to the existing C5-C6 group by using improved electrode technology for some muscles and by combining several upper extremity functions into a single neuroprosthesis. The new technologies that we will develop and implement in this proposal are: the use of nerve cuffs for complete activation in high tetraplegia, the use of current steering in nerve cuffs, imaging-based assessment of maximum muscle forces, denervation, and volume activated by electrodes, multiple degree-of-freedom control, the use of dual implants, new neurotization surgeries for the reversal of denervation, new muscle transfer surgeries for high tetraplegia, and an improved forward dynamic model of the shoulder and elbow. During this contract period, all proposed neuroprostheses will come to fruition as clinically deployed and fully evaluated demonstrations.

## Summary of activities during this reporting period

The following activities are described in this report:

- *Functional stimulation patterns for a high tetraplegia neuroprosthesis*
- *Implementation of a floating threshold algorithm for of an EMG controlled computer mouse emulator*
- *Surgical implantation of nerve cuff electrodes for an advanced upper extremity neuroprosthesis*
- *Percutaneous evaluation of nerve cuff electrodes in C5 tetraplegia*
- *Selection of muscles for stimulation in a C5 neuroprosthesis*
- *Selection of muscles for EMG recording and implantation sites in a C5 neuroprosthesis*
- *Feed-forward control of neuroprosthetic systems characterized by redundant muscles acting on multiple degrees of freedom*

## Overview

The activities in this quarter focused on the implementation of two implanted neuroprostheses covered under this contract: 1) the continued development of functional applications for the high tetraplegia neuroprosthesis; and 2) the implementation of an advanced upper extremity neuroprosthesis for C5-level tetraplegia that utilizes nerve cuff electrodes for shoulder and proximal arm function.

# Functional Stimulation Patterns for a High Tetraplegia Neuroprosthesis

*Contract section:*

E.1.a.ii. Model-based development of neuroprosthesis for high tetraplegia

## Abstract

Several functional stimulation patterns were developed for the individual with high tetraplegia who had received the dual-stimulator (24-channel) neuroprosthesis. In addition to modifications of the simulated-eating stimulation pattern that was discussed in the previous progress report (which involved elbow and shoulder movements), stimulation patterns were created for opening and closing of the hand and pronation and supination of the forearm. Once the stimulation patterns were developed, two of the subject's four myoelectric signals (MES) were used as command signals to control these patterns, allowing her to voluntary control her arm for the first time since her injury. A mode switch was investigated as a method of switching between the stimulation patterns.

Due to the subject's shoulder tightness, which limited external rotation and shoulder abduction, a mobile arm support was utilized to allow testing of the MES-controlled stimulation patterns in a more functional position.

## Methods and Results

In the previous progress report, a musculoskeletal model was used to develop proximal stimulation patterns that moved the upper arm and shoulder for a simulated eating task. This pattern was tested with the subject with high tetraplegia (C1 level injury on her right side) who has received the dual-stimulator (24-channel) neuroprosthesis. In this quarter, additional stimulation patterns were developed. Two patterns for the hand were created (see Figure 1). One was for a lateral grasp (for holding a key or a fork), while the other was for a palmar grasp (for holding a cup or a book). Similarly a stimulation pattern was developed for pronation and supination of the forearm (see Figure 2).

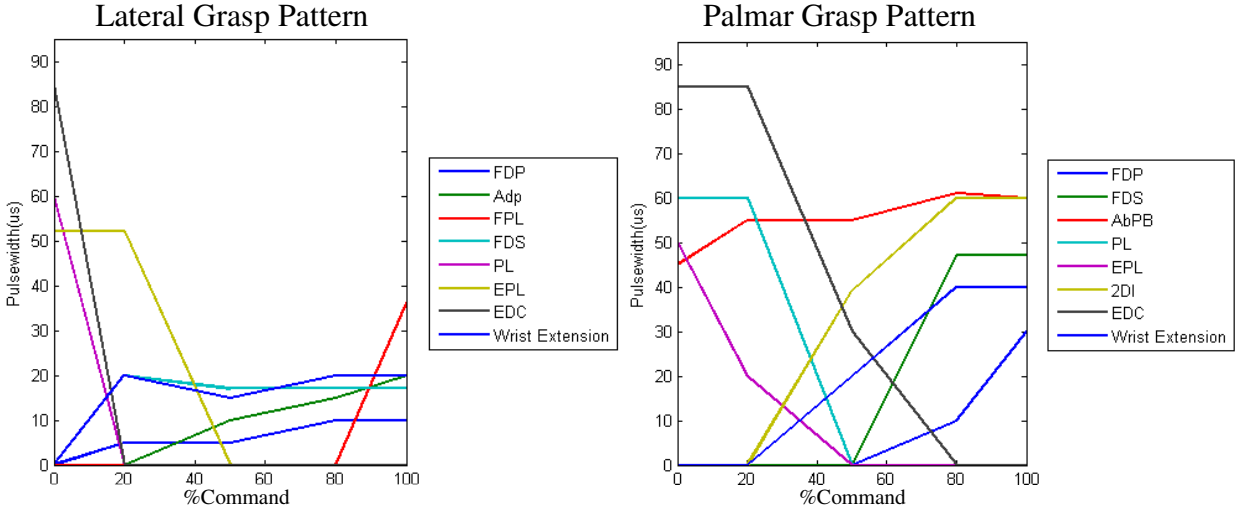


**Figure 1. Lateral and palmar grasp stimulation patterns.**

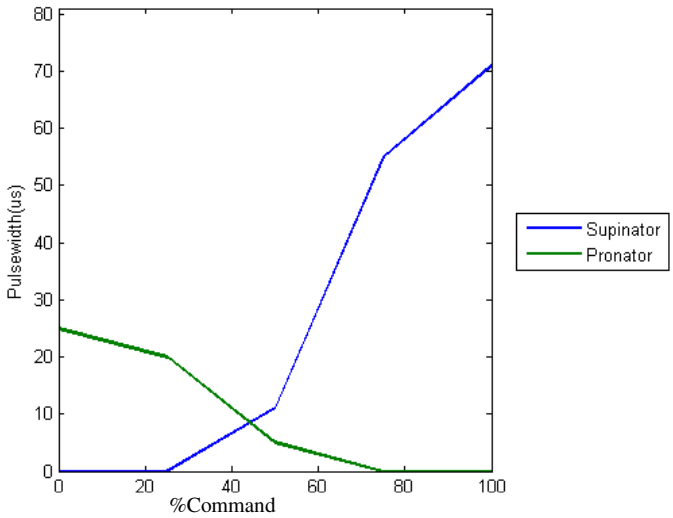


**Figure 2. Pronation/Supination stimulation pattern.**

With the high tetraplegia neuroprosthesis, there are four MES recording electrodes that can be used as control signals. In this subject there are MES electrodes on her left and right platysma muscles (in the neck), on her right auricularis muscle (behind the ear), and on her left trapezius muscle. It was decided to simplify her initial control technique by just using her left and right platysma MES signals. A control algorithm was set up that produces a command signal based on the difference between the left and right platysma signals. For example, to reach out she contracts her left platysma while relaxing her right platysma. This moves her command signal into the region of the stimulation pattern where the triceps and external shoulder rotators are stimulated, causing her arm to extend and move outwards (see Figure 3A). To bring her hand to her mouth, she contracts her right platysma while relaxing her left platysma. This moves her command signal into the region of the stimulation pattern where the biceps and internal shoulder rotators are stimulated, causing her arm to flex and move inwards (see Figure 3B).

**A)** **B)**

**Figure 3. A) Stimulated reaching controlled by neck MES signals. B) Stimulated arm flexion and internal rotation controlled by neck MES signals, allowing the subject to place a carrot in her mouth. A mobile arm support was used to overcome shoulder stiffness.**

The same control algorithm can be used to open and close the hand, and to pronate and supinate the forearm. Our initial plan is to have the subject use sequential movements to get her hand in the right position for a task, and to use a "mode switch" to go through the sequence steps. The first mode switch will be a button switch, so that the subject will start a task by using the command signal to move her arm to the desired object, then will press a button to switch to the pronation/supination pattern to orient the hand properly, then press the button again to switch

to controlling the hand grasp pattern. We are also investigating an MES-based mode switch as part of another NINDS contract (see Quarterly Progress Report #2 of the NINDS Contract N01-NS-5-2365). This MES-based mode switch uses a "double-jaw-clench" classifier algorithm to indicate when the subject wants to switch modes (see Figure 4).

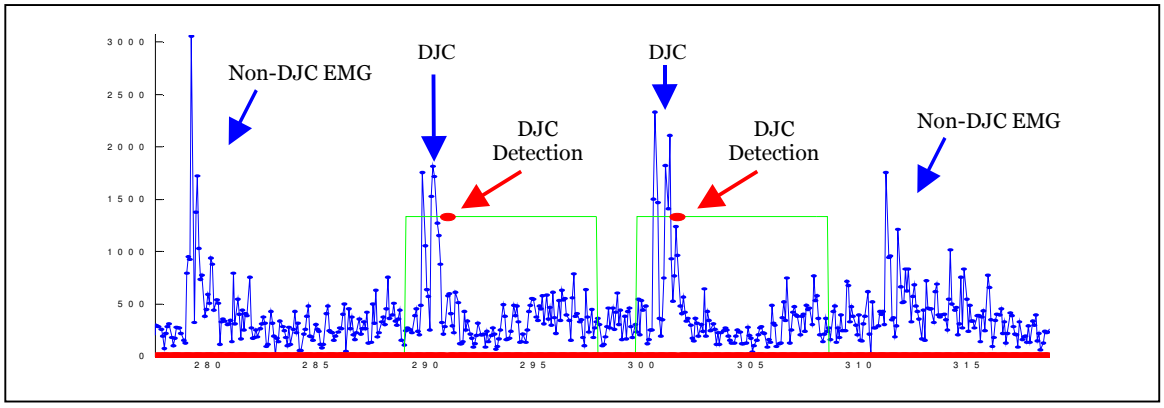


**Figure 4. Blue line is auricularis MES signal from FES subject. Green line indicates when a double jaw clench (DJC) cue went on. Red dots indicate when the classifier detected the DJCs in real-time.** ***Reprinted from Quarterly Progress Report #2 of the NINDS Contract N01-NS-5-2365*.**

The ability of the high tetraplegia subject to abduct and externally rotate her shoulder has been limited by spasticity and/or passive tightness in her shoulder. While these issues are being evaluated by her clinical providers, we have opted to use a mobile arm support to place her arm in a more functional position for the evaluations of these control methods and stimulation patterns (as shown in Figure 3).

### Next quarter

In the next quarter, we plan to further refine the stimulation patterns and MES signal control algorithm. We plan to implement the stimulation patterns with the button mode switch in a take-home system that will allow the subject to practice functional activities.

## Implementation of a Floating Threshold Algorithm for of an EMG Controlled Computer Mouse Emulator

*Contract Section:* E.1.a.iv. Command sources for High Tetraplegia

### Abstract

A software mouse emulator was implemented to translate incoming EMG signals via a serial port and convert these into mouse motion commands. This reduced the overall complexity of the system and made it more portable. The fixed threshold gated ramp was replaced with a floating threshold, which follows the natural drift of the resting EMG signal. This improved performance and increased the robustness of the system, minimizing the amount of recalibration required during operation.

## Methods

The mouse emulator has been simplified to a three function program that reads in the steady serial output from the stimulator controller and converts these signals into mouse commands. The user interacts with this software via the graphical user interface shown in Figure 5. The external single board computer is no longer required, though the modified mouse discussed in the previous progress report is still needed for button presses. The software has been compiled into a DOS based executable, accessible from the Windows desktop.

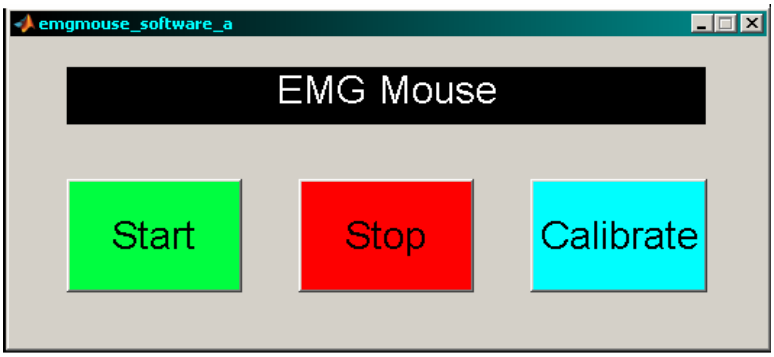


**Figure 5. Interface for EMG controlled mouse.**

*Algorithm*

The fixed threshold gated ramp has been replaced with a floating threshold gated ramp to better follow the natural drift of the EMG signal coming from the external stimulator controller. The floating threshold algorithm detects the voluntary-action threshold using the baseline resting signal and the pre-recorded range of the signal. The floating threshold is approximately 20% of the range of signal above baseline.

The resting baseline is detected by finding the lowest value seen by the system. This is reset every 30 seconds to account for any upward drift of the signal. This minimizes the amount of unintentional cursor drift, which can occur if the resting EMG level rises above threshold, to at most 30 seconds, after which the baseline is reset to the higher resting level. Decreases in the resting level are accounted for automatically by the software detecting the new lower value. The apparent effects of resetting the baseline every 30 seconds is negligible as the new baseline is recovered in approximately 0.01 sec (see Figure 6). .

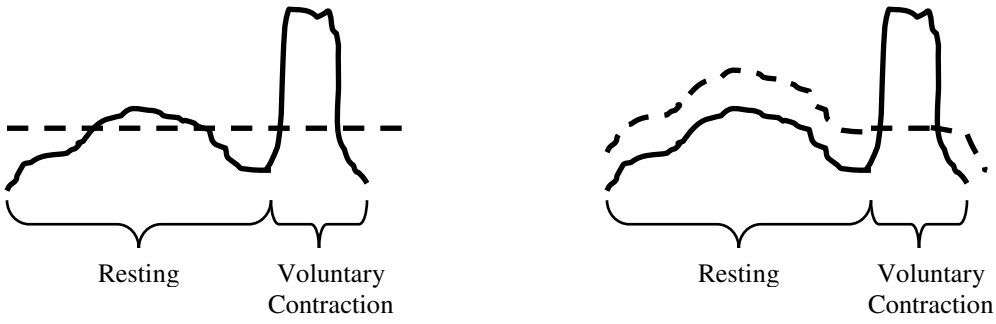


**Figure 6. Examples of fixed threshold (left) and floating threshold (right) where the solid line denotes the user signal and the dashed line indicates the threshold for movement initiation. Note that in the case of the fixed threshold, the resting state drifts above the pre-set threshold, which would create a false positive condition resulting in unwanted cursor drift. In contrast, the threshold in the figure on the right follows the contours of the baseline, but is still slow enough to capture the rapid transition of the voluntary user signal.**

*Operation*

The system uses the same muscle/command pairs discussed in the previous progress report, with the right and left platysma controlling left and right cursor motion, the left trapezius controlling upwards motion and the right auricularis controlling downwards motion.

The emulator software and graphical user interface (GUI) is launched from the Windows desktop. Upon launch, the user is presented with the GUI seen in Figure 5.

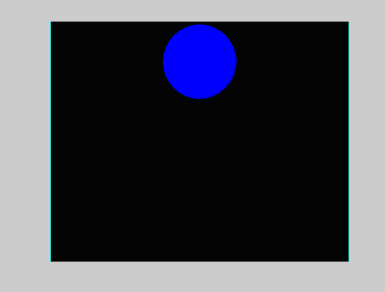

**Figure 7. Calibration screen with upwards resting target displayed.**

The system is first initialized by running the calibration routine, where the user is guided through resting and contracting states. Targets appear in a pop-up window in the center of the screen. The targets are show sequentially in each of the four directions (Figure 7). First the target is blue for 2 seconds to indicate a relaxed state, and then it turns green for four seconds to instruct the user to contract. The users's EMG signal is collected during this time and the range of each signal is calculated. The floating threshold is set to 20% of this range above the detected baseline.

To start the emulator, the green "Start" button (Figure 5) is pressed, which turns on EMG control of the cursor. Conventional mouse input is also still available during this time. To pause or stop EMG control, the "stop" button is pressed on the GUI. Recalibration is possible at any time during operation, but the emulator must be manually re-started following each calibration routine.

To move the cursor, the user contracts the muscle which corresponds to the desired direction. When the user's EMG signal is above the floating threshold, the cursor moves in the corresponding direction at a speed of 2000 pixels/sec. This speed was found to be the best trade off between rapid motion and end-point accuracy.

**Results**

In preliminary tests with a healthy subject using surface EMG signals, the average information transfer rate was increased by 47% (1.5 bits/sec compared to 0.71 bits/sec) using the floating threshold algorithm. When the mouse emulator was used by the subject with high tetraplegia, it has resulted in stable long-term operation, with little need to re-calibrate during operation. Most significantly, the amount of unintentional cursor drift has been dramatically reduced, greatly enhancing the operability of the mouse emulator.

**Next Quarter**

Quantitative evaluation of the floating threshold algorithm with the SCI subject will be performed in the next quarter and the results compared to previous fixed threshold experiments. Due to the ability of the floating threshold algorithm to detect and follow the baseline as it drifts in time, a variable velocity gated ramp is possible. This would produce cursor velocity that is proportional to the EMG signal to allow for more natural motion, as well as variable speed to either cross the screen rapidly, or make fine adjustments in cursor position. To this end, a variable velocity mouse emulator/evaluator is in the final stages of development and testing.

## Surgical Implantation of Nerve Cuff Electrodes for an Advanced Upper Extremity Neuroprosthesis

***Contract sections:*** E.2.a.ii.4.3 Implementation of advanced upper extremity neuroprosthesis

**Summary**

In this quarter, four nerve cuff electrodes were successfully implanted in the upper extremity and trunk of a subject with mid-cervical level tetraplegia. The electrode leads were connected to temporary percutaneous leads to allow the nerve cuff electrodes to be studied. Three weeks after surgery, the electrodes were tested and exercise was set up. After 4 weeks of exercise, the subject came in to the laboratory for the initial evaluation of the electrodes.

**Methods**

*"Improved C5/C6" neuroprosthesis candidate*

As stated in the previous quarter's progress report, the candidate selected for this study is 43-year-old white male who sustained a C4/C5 spinal cord injury from a diving accident in 1985. This candidate has C5-level function on both sides (little to no wrist extension, but can voluntarily activate his brachioradialis). Almost all of the targeted muscles in this study were able to be electrically activated. His right side is slightly stronger and therefore was chosen as the target for the neuroprosthesis.

In the first phase of the neuroprosthesis implantation, four nerve cuff electrodes were implanted, with the leads connected to percutaneous wires for external testing. The four nerves implemented were selected based on previous work in this Contract, including cadaver studies and simulations performed with a model of the shoulder. These four nerves are:

- Radial nerve – four contacts on the cuff could allow selective control of elbow extension, wrist extension, and finger extension.

- Thoracodorsal nerve – whole nerve stimulation for shoulder adduction and extension (latissimus dorsi).
- Long thoracic nerve – whole nerve stimulation for scapular abduction (serratus anterior).
- Suprascapular nerve – whole nerve stimulation for stabilizing the rotator cuff capsule and humeral rotation (supraspinatus, infraspinatus).

**Results**

*Radial nerve*

The radial nerve was exposed near the location where the nerve branches to the long head of the triceps. It was initially difficult to locate the radial nerve since this subject had an unusual radial nerve trajectory which went more anterior than a typical radial nerve. The nerve diameter was measured at 6 mm. We wanted to investigate whether the different contacts of the cuff electrode could selectively activate different portions of the radial nerve, so a 6 mm diameter, four-lead electrode was selected (one lead for each contact). We wanted to avoid stimulating the long head of the triceps (since it adducts the shoulder), so the cuff electrode was placed distal to the long head branch. The electrode was tested by stimulating each contact. Selective activation was observed, since one contact activated triceps without activating wrist extension, while one contact activated brachioradialis and wrist extensors without activating triceps. At the end of the surgery, each contact was stimulated and all four contacts were functional.

*Thoracodorsal nerve*

The thoracodorsal nerve was exposed and tested with a bipolar probe. The nerve diameter was measured at 2 mm, so a 2 mm diameter nerve cuff electrode was selected. The nerve cuff electrode was placed on a custom-designed double-hooked forceps (Figure 8) to facilitate wrapping the cuff around the nerve. The electrode was placed on the nerve and tested. Appropriate activation of the latissimus dorsi was achieved.

*Long thoracic nerve*

The long thoracic nerve was exposed and tested with the probe. The nerve diameter was measured at 2 mm, so a 2 mm diameter nerve cuff electrode was selected. The electrode was placed on the nerve and tested. Only a slight contraction of the serratus anterior was achieved at the highest stimulus parameters. The electrode was left on the nerve in case the lack of activation was due to an acute response to the surgical manipulation of the nerve.

*Suprascapular nerve*

The suprascapular nerve was exposed and tested with the probe. The nerve diameter was measured at 3 mm, so a 3 mm diameter nerve cuff electrode was selected. The electrode was placed on the nerve and tested. Appropriate activation of the infraspinatus and supraspinatus muscles was achieved.

*Tunneling leads and percutaneous connections*

The leads from all four cuff electrodes were tunneled to a site in the abdomen just under the ribs near where the stimulator will be placed. A connector incision was made, and each lead was connected to a percutaneous lead adapter. Each percutaneous lead was passed via an

angiocath through the skin at a location lateral to the connector site. After each percutaneous lead was tested to show electrical continuity to the cuff electrode, all the incisions were closed.

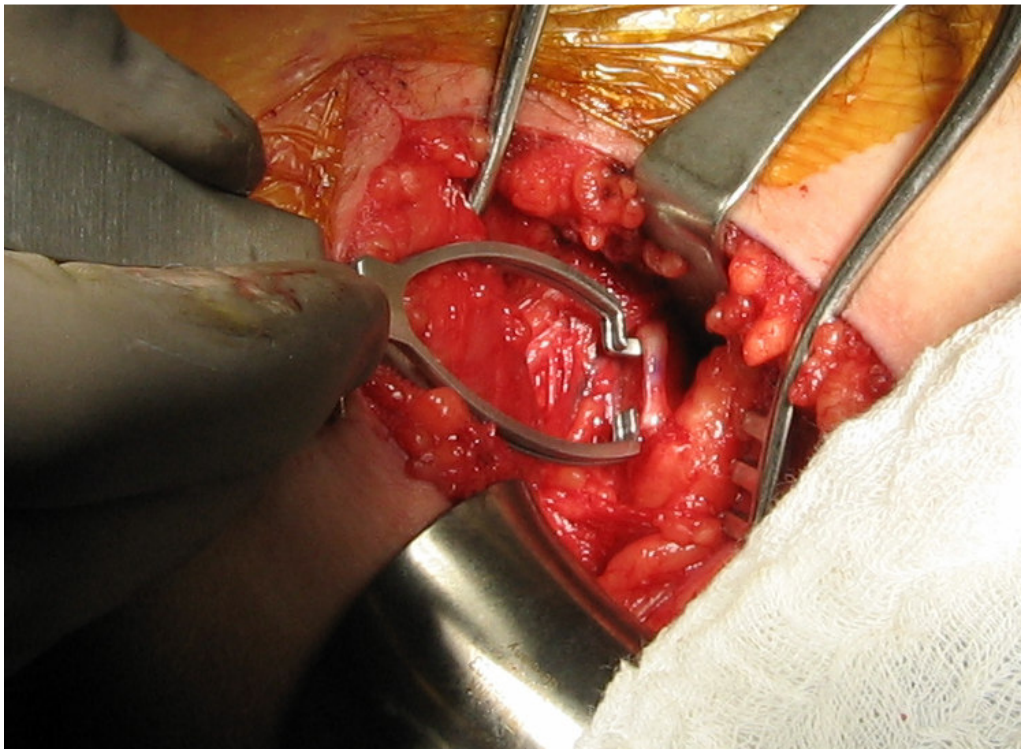

**Figure 8. Nerve cuff electrode being held by a double-hooked forceps prior to being placed around the thoracodorsal nerve.**

*Post-surgical care*

The incision sites were bandaged and the shoulder was stabilized with a velpeau restrictive dressing. X-rays were taken of the arm and shoulder (see Figure 9). Pins were crimped onto the percutaneous leads and placed into a connector block so that a cable could easily be plugged into the leads (see Figure 10). The exit site was covered with a bandage. The shoulder was stabilized for 3 weeks.

*Electrode testing and exercise setup*

After the 3 week stabilization period, the electrodes were characterized and exercise stimulation patterns were started. During testing, one of the four channels (#3) of the radial nerve cuff did not produce a response. We looked at the stimulus waveform on an oscilloscope and it had the characteristic waveform shape for an open circuit. The suprascapular nerve cuff electrode also displayed an open-circuit waveform. The long thoracic nerve continued to produce no response in the serratus anterior. However, it did not have a high impedance or open-circuit waveform, indicating that current was getting to the nerve, but no activation was occurring. The other cuff contacts (radial nerve contacts #1, 2 and 4, and thoracodorsal nerve) all got good responses from the target muscles. The four functional contacts were programmed into an exercise pattern in a portable stimulator for the subject to take home and use for exercise.

**Figure 9. X-ray showing 3 of the 4 nerve cuff electrodes (circled).**

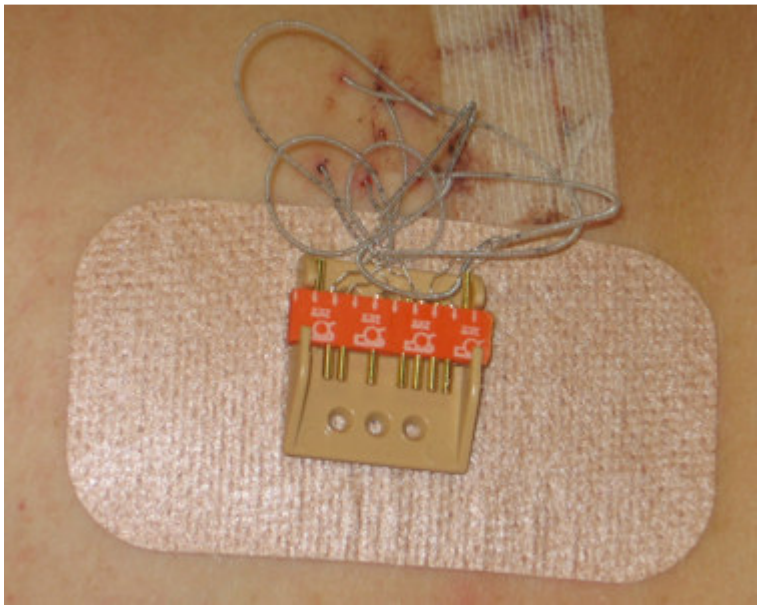

**Figure 10. Percutaneous leads in a connector block.**

*Initial electrode testing visit*

After four weeks of exercise, the subject came back to the lab to characterize the cuff electrodes. Results of these tests are included in the next section of the progress report. It was observed that the suprascapular nerve cuff electrode was now working, and no longer displayed an open-circuit waveform. The connector site was manipulated to see if it was an intermittent connection, but the electrode functioned consistently throughout the testing.

## Next Quarter

The subject will exercise with the cuff electrodes for five more weeks after the initial testing visit. During this period, the subject will come to the laboratory two more times to have the nerve cuff electrodes evaluated, and to prepare for the surgical implantation of additional electrodes and stimulators. During these surgeries, the percutaneous leads to the nerve cuff electrodes will be removed, and the electrodes will be connected to an implanted stimulator-telemeter. Intramuscular electrodes for his trunk will also be implanted and connected to this stimulator. A second stimulator-telemeter will also be implanted, with additional intramuscular electrodes being inserted into his forearm and hand muscles to form an advanced upper extremity/trunk neuroprosthetic system.

# Percutaneous Evaluation of Nerve Cuff Electrodes in C5 Tetraplegia

***Contract section:***

E.1.a.i.4.4. Evaluation of single and multicontact cuffs via percutaneous leads

**Abstract**

Four percutaneous spiral nerve cuff electrodes were implanted in a second subject on May 2, 2006. This second subject has C5 tetraplegia (see details in previous section). Spiral nerve cuff electrodes were implanted on four upper extremity nerves and the leads were passed across the skin at the side to allow for external hook up. The purpose of the percutaneous testing phase of this project is to do a more detailed evaluation of nerve cuff electrodes than is possible using an implanted system. We will be evaluating the stability, selectivity and force production capabilities of the electrodes. Data from the implant surgery and the first follow up visit are included here.

## Methods

*Implant*

Electrodes were implanted on four upper extremity nerves. A four channel, selective electrode (Figure 11C) was implanted on the radial nerve, and single channel electrodes were implanted on the suprascapular (Figure 11B), long thoracic and thoracodorsal (Figure 11A) nerves. The single contact electrodes were used on nerves with a 2 mm diameter since fabrication with all four contacts was not feasible. During the implant surgery, recruitment curves were generated by stimulating each contact and recording the EMG signals from the corresponding muscles using needle EMG recording electrodes. Following the cuff electrode implantation, the subject's arm was immobilized for three weeks with a sling and swab to allow for electrode encapsulation.

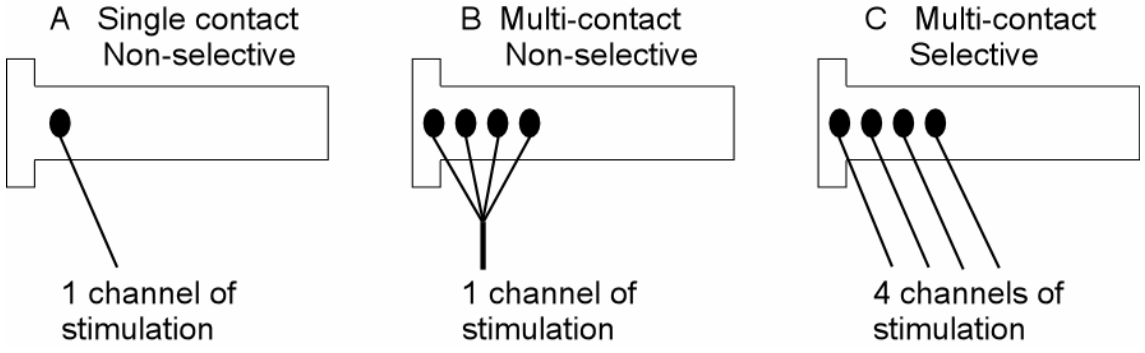


**Figure 11. Schematic of non-selective and selective electrodes. Non-selective electrodes have all four contacts tied together, resulting in a single channel of stimulation. Selective electrodes have four individually controlled contacts, resulting in four channels of stimulation.**

*Exercise*

Following the three week immobilization period, threshold and supramaximal activation values were determined for each electrode to verify muscle contraction and establish an exercise regime. During this first stimulation session, the current intensity was slowly increased for each channel of each electrode. Once the threshold and maximum values were determined, an

exercise pattern was set-up that cycled stimulation between the shoulder and the arm. The subject was instructed to exercise at home for two hours a day.

*Moment Measurements*

Tetanic stimulation (12 Hz) was used to measure the force production capabilities of the muscles at 7 weeks post implant. To measure shoulder moments, the subject was placed in a setup consisting of a JR3 force and moment transducer attached to the endpoint of the humerus with the elbow bent to 90º. The shoulder was position at 45º of abduction and 0º of horizontal flexion. To measure elbow, wrist, and finger moments, the subject was placed in a device that consisted of 4 individual four bar linkage transducers, one for the elbow and wrist and one for each of the first two fingers (see previous progress report for figure). Measurements were made at four pulse width values for each contact.

*Electromyography Recordings*

Surface and percutaneous EMG recordings were used to evaluate recruitment and selectivity of each nerve. Twitch recruitment curves were generated using only monopolar stimulation this quarter but current steering (simultaneous, subthreshold activation of adjacent contacts) will be used in the future.

**Results**

*Electrode Positional Stability*

To determine if the electrodes move during and after the surgery, the recruitment curves generated intraoperatively were compared with curves generated 7 weeks post implant (Figure 12). At both times, stimulation of channel 2 resulted in triceps activation before the other muscles while stimulation of channel 4 resulted in activation of brachioradialis first and triceps last. This indicates that intraoperative testing is a valid predictor of chronic performance.

*Thresholds*

The nerve activation thresholds appear to be stable between the time of implant and 7 weeks post implant. The average intraoperative threshold for the three radial nerve contacts was 24 ± 9 nC and at 7 weeks post implant it was 19 ± 10 nC. This is within the range reported in previous quarterly progress reports. Threshold calculation was not done for the other nerves at this point in the testing.

*Selective Activation*

Monopolar cathodic stimulation selectively activated the triceps on the radial nerve both intraoperatively and 7 weeks post implant. (Figure 12-top row) Current steering (simultaneous subthreshold anodic stimulation of adjacent contacts) will be used in future testing session to attempt to improve the selectivity of the triceps as well as to isolate additional muscles from the radial nerve.

*Moment Production*

Moment measurements were made at 7 weeks post implant. Moments will also be measured at 9 and 11 weeks to address the effects of exercise and verify that there is no loss of strength. The moments recorded at each pulse width are shown in Figures 13 and 14.

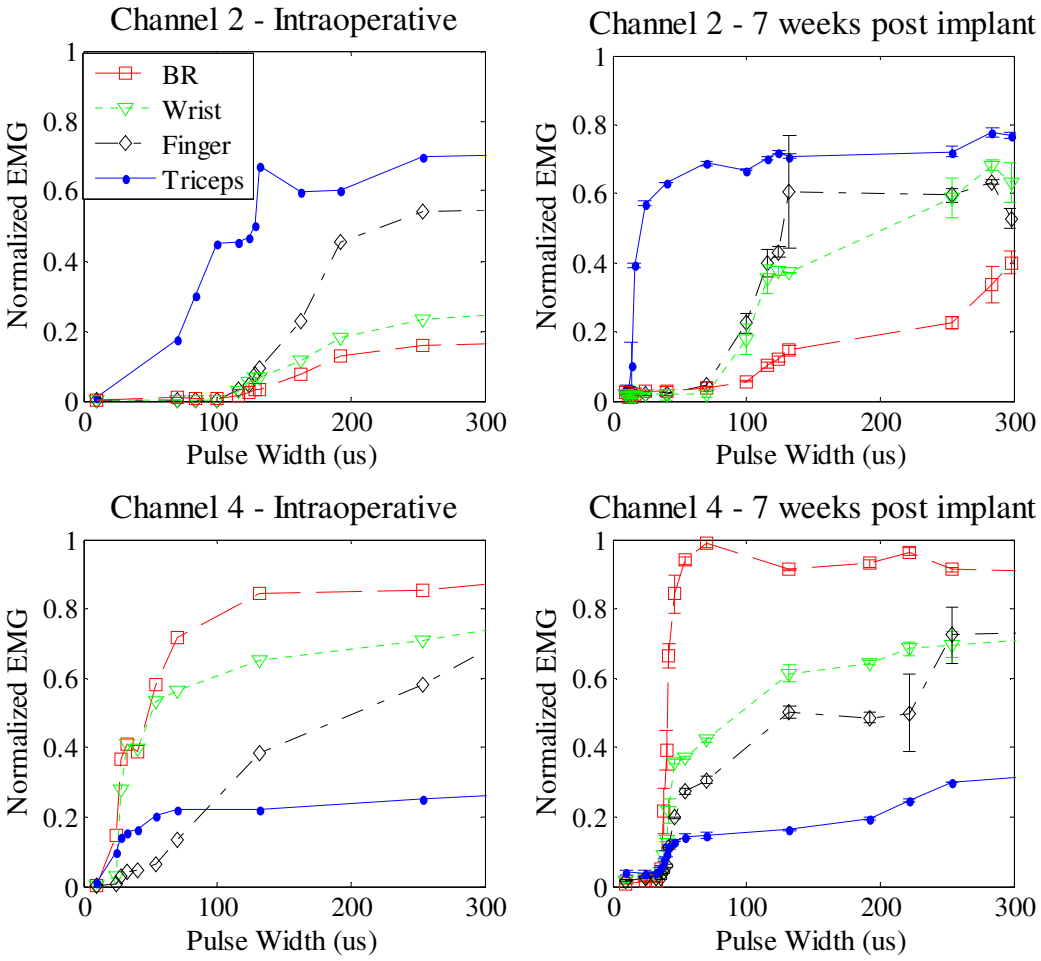


**Figure 12. Comparison of radial nerve electrode selectivity 7 weeks post implant to the selectivity recorded during the implant surgery. Channel 2 activates triceps first in both cases and channel 4 activates brachioradialis first and triceps last in both cases.**

## Next Quarter

The percutaneous testing phase is currently in progress. Experiments will continue until July 25th when the subject will receive a full upper extremity system, including trunk electrodes. The percutaneous connectors will be removed and the electrodes connected to implanted stimulators.

Specific items that will be studied next quarter are:

- Effects of current steering on selectivity
- Trends of joint moments over time
- Stability of nerve activation thresholds over time

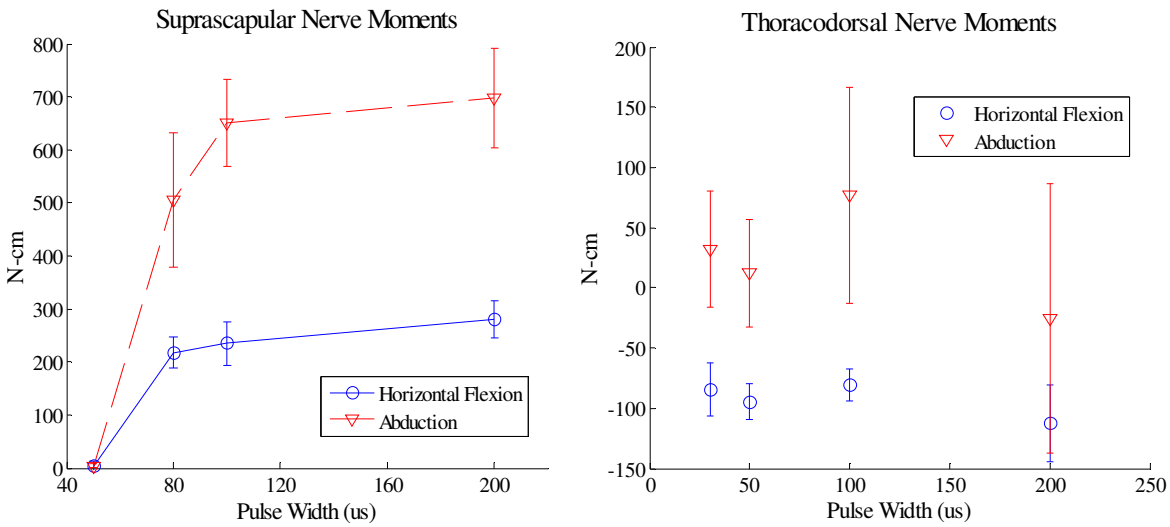


**Figure 13. Joint moments measured from axillary and musculocutaneous nerve stimulation at 7 and 9 weeks post implant. Pulse amplitude was 0.8mA for all pulse widths**

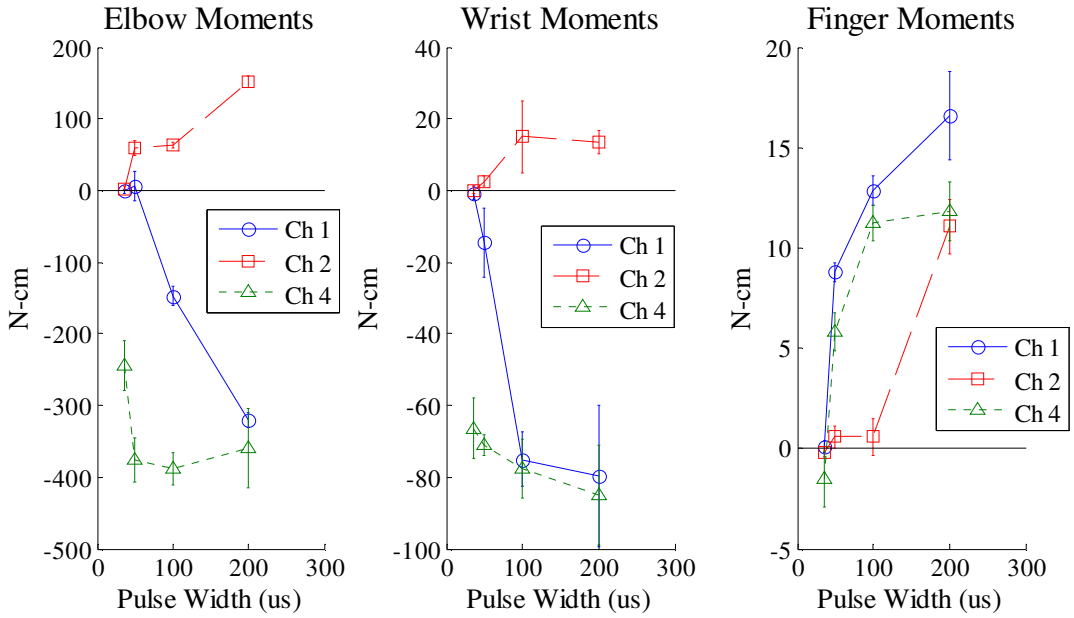


**Figure 14. Joint moments measured from radial nerve stimulation at 7 weeks post implant. Positive Y is extension and negative Y is flexion.**

# Selection of Muscles for Stimulation in a C5 Neuroprosthesis

***Contract section:***

E.2.a.ii.4.3. Implementation of advanced upper extremity neuroprosthesis

**Abstract**

We adjusted a computational model of the human upper extremity to reflect the condition of our recruited subject with C5 tetraplegia, and used simulation results to determine a subject-specific optimal set of candidate muscles for FES. This information was used to guide the research team of surgeons, clinicians, and engineers in preparation for the implantation surgeries.

## Methods

*Model adjustment to reflect the condition of our subject with C5 tetraplegia*

A manual muscle test (MMT) and an electrical excitability test (EET) provided information about the condition of the subject's arm musculature. These tests told us which muscles had enough voluntary control and which muscles were paralyzed but not denervated (necessary condition for electrical stimulation). The subject-specific muscle strengths provided by the MMT combined with the known nerve root innervation were used to reduce the maximum force that each muscle could produce. This reduction was included during the model description before performing inverse dynamic simulations. Additionally, we provided some muscles with a 50% of maximum force generation capability simulating the gross action of electrical stimulation.

*Use of model simulation results to select a candidate set of muscles*

We have a database of able bodied movements that we are interested in restoring in this population. These include reaching movements above and across the workspace and basic activities of daily living (ADL) such as grooming, eating, drinking, etc. We used this kinematic data as inputs and performed various inverse dynamic simulations where muscle activations are the output of the simulations. The candidate muscle set was chosen in two stages. First, we ran simulations where there was no reduction in the maximum muscle forces (i.e. able-bodied simulations) which provided an approximation of the maximum required muscle activations for the type of movements we want to restore. We compared this maximum activation for able-bodied simulations to our subject's C5 tetraplegic muscle condition and determined which muscles had a greater deficit to overcome with FES. Second, we ran more inverse simulations using different sets of reduced muscle strengths (C5 tetraplegic voluntary musculature + FES muscles) and compared the failure rate of the simulations for different conditions. The simulations fail when there is not enough force to balance the joint torques or when the stability of the glenoid is compromised. We simulated (i) a set with no FES (C5Only), (ii) one that included the muscles activated by the cuff electrodes selected for implantation (C5+Cuff) and (iii) another one that added the candidate muscle-based electrodes to the cuff set (C5+Stim). These simulations provided important information to assess if our set of target muscles for electrical stimulation would be enough for the expected functional outcomes of this neuroprosthesis.

**Results**

Table 1 shows the MMT test, the EET test, and the muscle reduction for our recruited subject. In the muscle reduction column, a one will correspond to full able bodied force generation capability. The fourth column shows the maximum able-bodied muscle activation required for all the movements from the kinematic database. Additionally, the muscles have been ranked according to the able-bodied-to-C5 reduction ratio so the firsts in the lists represent the muscles with the greatest deficit to overcome. Triceps, Pectoralis Major, Pronators, Serratus Anterior, Infraspinatus, Coracobrachialis and Subscapularis are some of the muscles to be considered.

**Table 1. Manual Muscle Test (MMT), Electrical Excitability Test (EET), Muscle reduction for model (Red.), and maximum able-bodied muscle activation required (AbMax)**

| | MMT | EET | Red. | AbMax |
|---|---|---|---|---|
| Pectoralis Minor | | | 0.00 | 0.00 |
| Triceps Long Head | **0** | | 0.00 | 0.11 |
| Pectoralis Major Thoracic | **0** | **4** | 0.00 | 0.18 |
| Triceps Medial Head | **0** | **4** | 0.00 | 0.65 |
| Triceps Lateral Head | **0** | **4** | 0.00 | 0.35 |
| Anconeus | | | 0.00 | 0.22 |
| Pronator Quadratus | **1** | **4** | 0.01 | 0.44 |
| Pronator Teres Hum-Rad | **1** | | 0.01 | 0.11 |
| Pronator Teres Uln-Rad | **1** | | 0.01 | 0.05 |
| Pectoralis Major Clavicular | **1** | **4** | 0.09 | 0.28 |
| Coracobrachialis | **3** | | 0.08 | 0.23 |
| Subscapularis | **2-** | | 0.14 | 0.40 |
| Serratus Anterior | | **0** | 0.16 | 0.43 |
| Infraspinatus | **4** | | 0.28 | 0.74 |
| Supinator Hum-Rad | **4+** | | 0.31 | 0.53 |
| Brachialis | **4+** | | 0.43 | 0.64 |
| Teres Minor | **4** | | 0.28 | 0.41 |
| Deltoid Clavicular | **3+** | | 0.23 | 0.27 |
| Deltoid Scapular | **4** | | 0.28 | 0.32 |
| Trapezius Scapular | **3+** | **4** | 0.35 | 0.38 |
| Supraspinatus | **4+** | | 0.54 | 0.52 |
| Biceps Short Head | **4+** | | 0.43 | 0.37 |
| Brachioradialis | **4** | | 0.38 | 0.31 |
| Trapezius Clavicular | **4** | | 0.40 | 0.25 |
| Rhomboids | **4** | **4** | 0.40 | 0.21 |
| Biceps Long Head | **4+** | | 0.43 | 0.20 |
| Levator Scapulae. | | | 0.50 | 0.05 |
| Teres Major | **1** | | 0.02 | 0.00 |
| Latissimus Dorsi | **1** | **4** | 0.01 | 0.00 |

In the second set of simulations we performed simulations with three different sets of muscles:

1. C5 Only: Subject's C5 tetraplegic condition with no FES
2. C5+Cuff: Radial Nerve (Triceps), Long Thoracic (Serratus Anterior), Thoracodorsal (Latissimus Dorsi) and Suprascapular (Infraspinatus and Supraspinatus).
3. C5+Stim: Cuff electrodes + Rhomboids, Pectoralis Major and Pronators

Table 2 shows the percentage of failure of all the trials simulated. The second column corresponds to movements where a 3 kg weight was added at the end point to simulate the presence of an object in the hand. Generic C5 corresponds to a typical C5 tetraplegic condition.

The selected stimulation set was able to reduce the percentage of failure of 31 trials that included different movements which we intend to restore to 4% when no weight was added and to 48% when the weight was added to the simulation. This provides evidence that the selected muscles for stimulation will be good enough to increase the reaching capacity of our subject to overhead and across the midline areas of the workspace. This muscle set helped the research team to select the final implementation for the neuroprosthesis implant.

**Table 2. Percent Failure for Simulated Trials**

| | % Failure | |
|---|---|---|
| | no weight | with weight |
| Generic C5 | 74.81 | 100.00 |
| C5 Only | 33.90 | 99.97 |
| C5 +Cuff | 8.41 | 87.49 |
| C5 + Stim | 3.99 | 48.32 |

**Next Quarter**

In the next quarter we will report the initial tests of the implanted system.

## Selection of Muscles for EMG Recording and Implantation Sites in a C5 Neuroprosthesis

***Contract section:***

E.2.a.ii.4.1. EMG-based shoulder and elbow controller

**Abstract**

Model-based analysis and surface EMG recordings were used (i) to verify if the targeted muscles were a good selection, (ii) to select which head of the selected muscle to use for the implanted EMG and (iii) to evaluate the specific implantation sites for the electrodes.

**Methods**

We targeted five muscle groups for our initial evaluation of EMG control sources. These were trapezius, deltoids, biceps, brachioradialis and extensor carpi radalis longus (ECRL).

*Modeling*

In the musculoskeletal model of the upper extremity, each muscle is composed of several elements due to its wide origins and different lines of action. After running inverse dynamic simulations, we obtained muscle activations for each of these elements. We used this outcome to evaluate which elements of each of the candidate muscles for EMG recordings were "most active" and thus identify a target location for the electrode. The "most active" element was quantified as the area under the curve of the rectified and 8Hz low-pass filtered signal. Additionally we performed a multi-input multi-output frequency domain system identification to find the correlation between the target input muscles and the selected stimulation muscle set. The procedure generated frequency responses and the partial-coherence (0-5Hz) of each input to each of the outputs was averaged for each input target muscle. The muscles were finally ranked

according to this partial coherence calculation. This allowed us to confirm that the initial set of candidates was going to be an adequate selection to predict the muscle stimulation levels of the paralyzed muscles that will receive FES.

*Testing*

We recorded surface EMG from the different portions of the candidate muscles suggested by the simulations. In these tests the subject was asked to perform different movements (e.g. raise the shoulder, retract the scapula, abduct the arm, flex the elbow, cover the workspace, etc). The goal of these recordings was to confirm the voluntary control over the portion of the muscle recorded.

**Results**

*Modeling*

Figure 15 shows the elements of the trapezius, deltoids and biceps that were most active (arrows) during the simulations. The upper trapezius, the middle deltoid and the short head of the biceps were active during most of the movements recorded, and thus were considered as target locations for the implanted EMG electrodes.

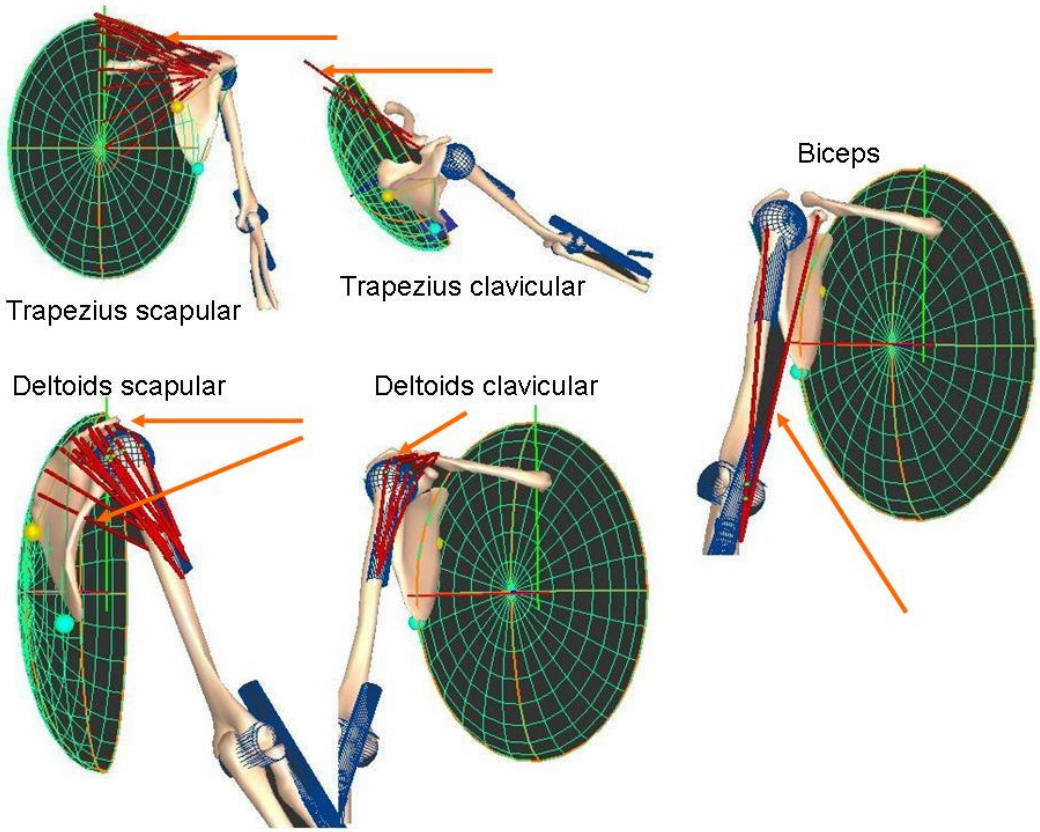


**Figure 15. Selection of most active elements from model simulations**

Table 3 shows the results of the system identification technique. The average partial coherence between 0-5Hz was obtained for each input/output muscle pair and then all the output

muscles were added for each input muscle. Biceps short head, trapezius scapular portion and deltoid clavicular portion were ranked first having strong coherence with muscles such as the serratus anterior, the infraspinatus and the clavicular portion of the pectoralis major.

**Table 3. System Identification Results**

| Rank | Muscle | Pcoh avg 0-5Hz | Output muscle contribution |
|---|---|---|---|
| 2 | Trap Scapular | 1.4719 | SerrAnt(0.76), InfrSpin(0.58) |
| | Trap Clavicular | 0.2789 | |
| | Deltoid Scapular | 0.2122 | |
| 3 | Deltoid Clavicular | 0.8678 | SerrAnt(0.25), PecM-Cl(0.28) |
| | Biceps LH | 0.7192 | SerrAnt(0.22), InfrSpin(0.35) |
| 1 | Biceps SH | 1.7379 | |
| | BrachioRadialis | 0.2532 | |

*Testing*

Figure 16 shows a series of pictures with the approximate locations of the target muscles and an example of surface recordings when the subject is raising the arm. The locations highlighted in the figure were selected as target locations for the electrodes. Upper trapezius, middle deltoid, short head of the biceps and ECRL were selected to be implanted with recording EMG electrodes. ECRL has been used in the past for users to control opening and closing of the hand. Brachioradialis gives an equivalent signal and it will be transferred to the ECRB to

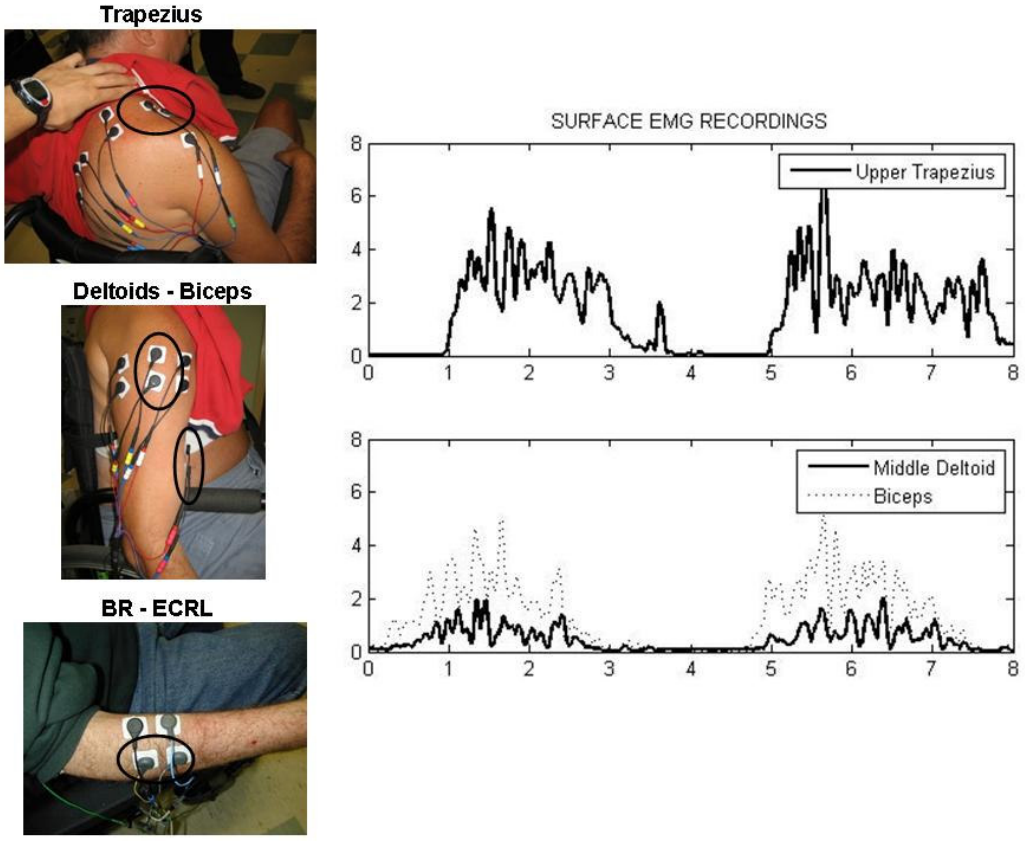


**Figure 16. Surface EMG recordings**

increase his voluntary wrist extension. Trapezius, deltoids, and biceps will be evaluated as control signals to determine the stimulation levels of the shoulder and elbow muscles selected for FES (i.e. pectoralis major, pronator quadratus, serratus anterior, triceps, supraspinatus, infraspinatus and rhomboids).

**Next Quarter**

In the next quarter we will report the signal characteristics of the implanted muscles with EMG electrodes.

## Feed-Forward Control of Neuroprosthetic Systems Characterized by Redundant Muscles Acting on Multiple Degrees of Freedom

**Contract section:**

E.2.a.ii. Simultaneous and natural control of multiple arm and hand functions.

**Abstract**

We created a time-invariant forward neural network model (system model) of a human thumb using time-varying, coupled and redundant data relating muscle stimuli to muscle outputs. We used the forward model to average the input-output data and thus eliminate its time-variance. We then chose unique input-output data from the time-invariant set to optimize specific performance criteria, such as minimum co-activation, allowing us to eliminate redundancy and thus obtain a unique solution. We trained an inverse-model, static, feedforward, artificial neural network controller with these optimal input-output data. We tested the controller isometrically with seven able-bodied individuals.

**Background**

Most movements require coordination of multiple muscles crossing multiple degrees of freedom. In neuroprostheses, this is usually achieved by mapping a command signal to the activation levels of the electrically stimulated muscles to achieve the desired movement kinetics/kinematics. Artificial neural networks (ANNs) offer the potential of automating the creation of these maps since they can learn complicated nonlinear multidimensional relationships on the basis of clinically measured input-output data. To create an inverse controller, the ANN maps must invert the input-output relationship, which is nearly always non-unique due to biological variability in muscle responses and the greater number of muscles than degrees of mechanical freedom in the limbs.

We previously developed a method for implementing feedforward neuroprosthetic controllers for musculoskeletal systems with multiple degrees of freedom and complex mechanical interactions [Lujan and Crago 2004]. Our tests showed that controller performance was poorer than we expected, and we attributed the poor performance to redundancy of the data used to train the controllers. In other words, if left unrestricted, controller implementation may result in an unsuitable inverse. We addressed this ANN training problem by first training an intermediary ANN that models the forward input-output properties of the system being controlled, then using this model to create unique and optimized data to train the inverse ANN controller [Kirsch et al. 2005]. Our present work involves obtaining this unique inverse solution

and using it to train a controller capable of providing independent control of coupled degrees of freedom.

We obtained IRB approval for surface stimulation using an in-house surface stimulator that can be controlled in real-time with a computer. We tested our controller isometrically with seven able-bodied individuals.

**Force Measurement Apparatus**

The mechanical characteristics of the thumb, such as coupled degrees of freedom (i.e., abduction/adduction-flexion/extension) actuated by redundant muscles (i.e., more than one muscle adduct and flex the CMC joint), allow us to study mechanical redundancy and coupling while controlling the forces at the tip of the thumb (Figure 17).

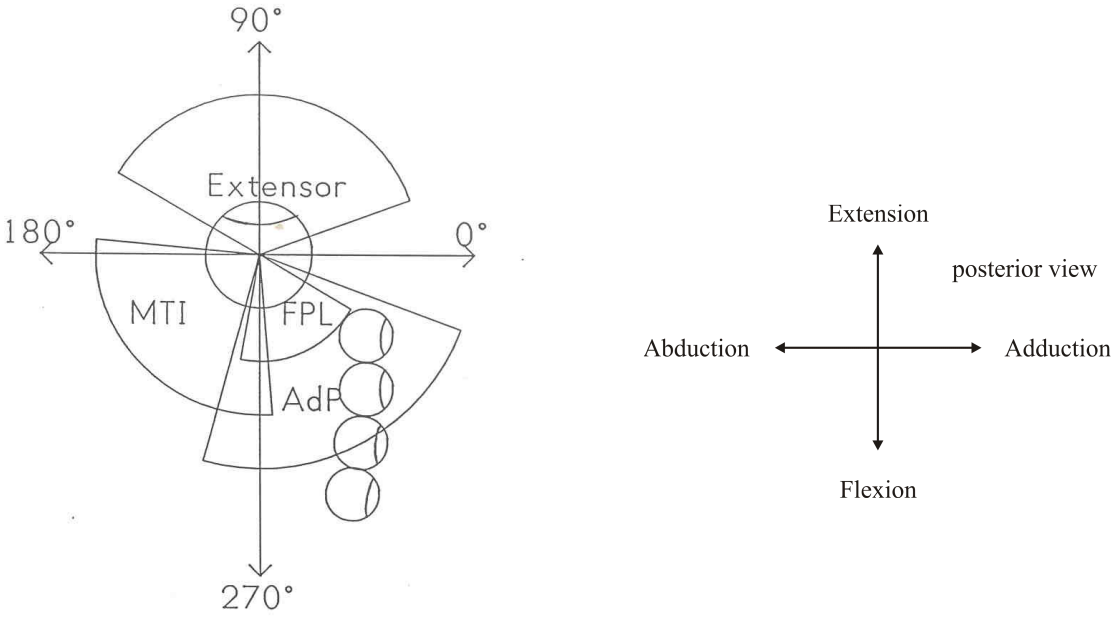


Posterior view

**Figure 17. Force directions for the extensor pollicis longus (EPL), abductor pollicis brevis (AbPB), adductor pollicis (AdP), and flexor pollicis brevis (FPL) in a right hand [Kilgore 1987].**

We used a 3-axes force/moment JR3 transducer (JR3, Woodland, CA) to measure the forces at the tip of the thumb along the flexion/extension adduction/abduction planes. The force sensor was mounted onto a camera tripod, which was attached to a wood platform with adjustable height (Figure 18).

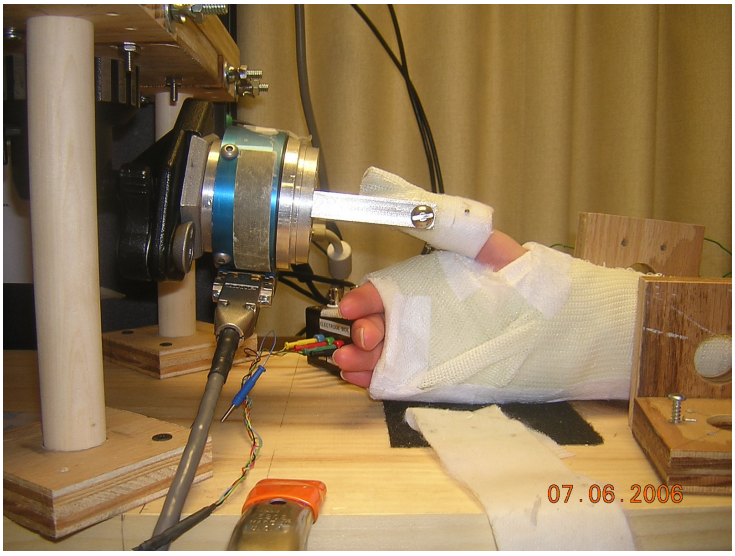


**Figure 18. The combination of tripod and platform allowed multiple positioning of the thumb with respect to the transducer and adjustments for different hand sizes.**

## Experimental Protocol

We tested our methodology on seven able-bodied individuals using skin surface stimulation. The areas identified for electrode placement were cleaned with alcohol to remove skin impurities and electrode gel was applied to further reduce skin impedance.

The hand and thumb were placed inside custom-made casts to prevent unwanted rotation of the wrist and interphalangeal (IP) joints. The thumb cast was attached to the JR3 through a pin joint to eliminate moments at the tip. Adjustable wood restraints stabilized the forearm by preventing pronation/supination. Velcro strips glued to the cast and wood platform prevented sliding of the arm as well as elevation of the elbow and wrist. The subject was instructed to relax and avoid any voluntary movements of the arm, wrist, and fingers.

Activation thresholds were determined by incrementally stimulating each muscle from 0 to 200 microseconds and measuring the end-point forces. Saturation/spillover thresholds were defined as those pulsewidths where unwanted spillover occurred (observed as undesirable muscle contractions), stimulation became painful or end-point forces reached a plateau. Muscles were stimulated at maximum pulsewidth (200 microseconds) for two periods of five seconds (with three seconds of rest in between) to reduce the effect of muscle warm up after long periods of no stimulation.

## Data Collection

Typically six, four, and six equally-spaced stimulation pulsewidths were selected from activation to saturation thresholds for the extensor pollicis longus (EPL), abductor pollicis brevis (AbPB) and adductor pollicis (AdP) muscles, respectively. The four pulsewidths were assigned to the weakest muscle, as determined by the force magnitude under maximum stimulation. All possible pulsewidth combinations were computed and randomized. Muscles were stimulated at 50 Hz for two seconds and allowed to recover for ten seconds for each pulsewidth combination. Thumb forces were averaged over the last second (after reaching steady-state) to obtain the time-varying data set for system model training.

The forces collected in each experiment (Figure 19) indicate good force ranges over which we might be able to control end-point force production. These force ranges were explained by summation of the individual force vectors produced by each muscle.

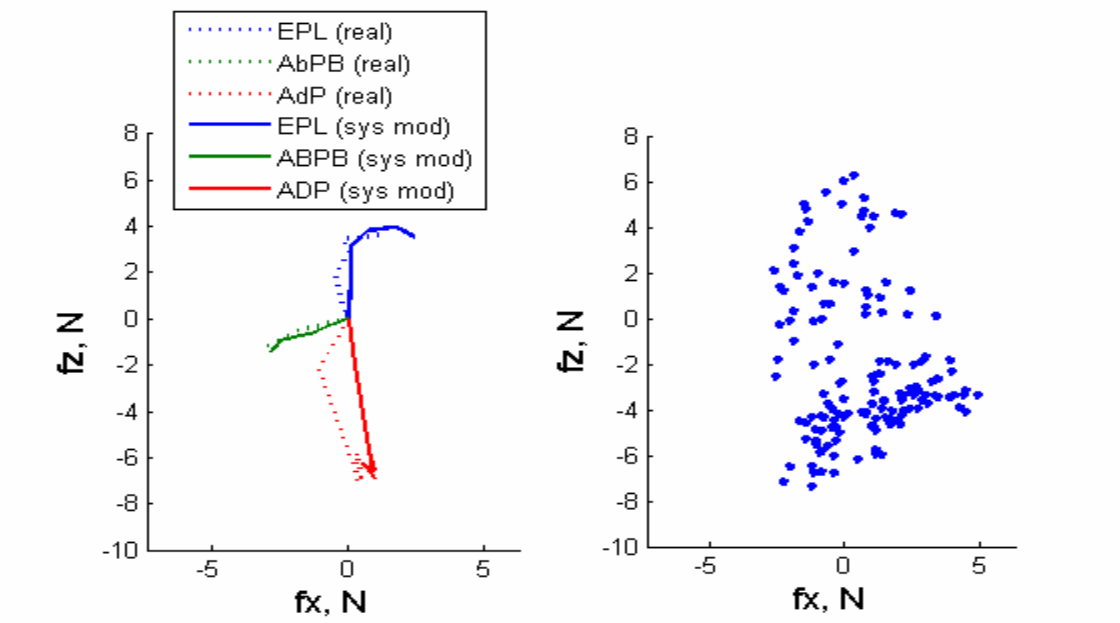


**Figure 19. Clinical data measured in experiment 7 during stimulation of three muscles: extensor pollicis brevis (EPL), abductor pollicis brevis (AbPB), and adductor pollicis (AdP) (right), and force vectors for the real data and trained system model (left).**

## System model

The system model was trained on these time-varying input-output data, and time invariant data was created. To determine the number of hidden neurons for both networks, we systematically varied the number of hidden neurons for the system model and inverse controller from four to seven neurons while the RMS fitting and prediction errors were measured. Training and testing of the system model and inverse controller was repeated ten times at each combination of neurons. The smallest errors were measured when the system model and inverse controller had twenty hidden neurons each, in contrast to the six and twenty five neurons, respectively, obtained for the simulation data.

In most cases, the forces generated by each muscle in the system model matched those of the real musculoskeletal system (Figure 19, left) for the same set of stimulus parameters. The system models were capable of eliminating data variability while still modeling nonlinearities of the real muscles, such as those resulting from spillover, which strongly suggests that we were able to obtain a good representation of the real musculoskeletal system in most cases.

## Optimization

The time-invariant data were optimized to reduce muscle activations and find a unique solution.

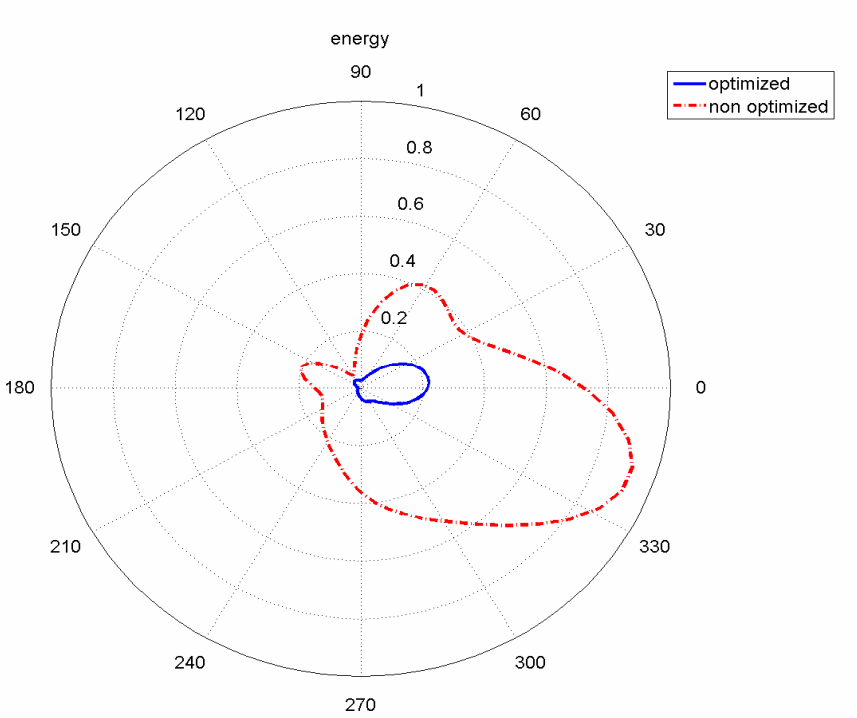


**Figure 20. Energy for non-optimized (dashed line) and optimized (solid line) pulsewidths for experiment 7.**

Optimization of the muscle activations, defined as the percentage fraction of muscle active, reduced the overall amount of energy used (Figure 20) while still achieving the required force targets (Figure 21).

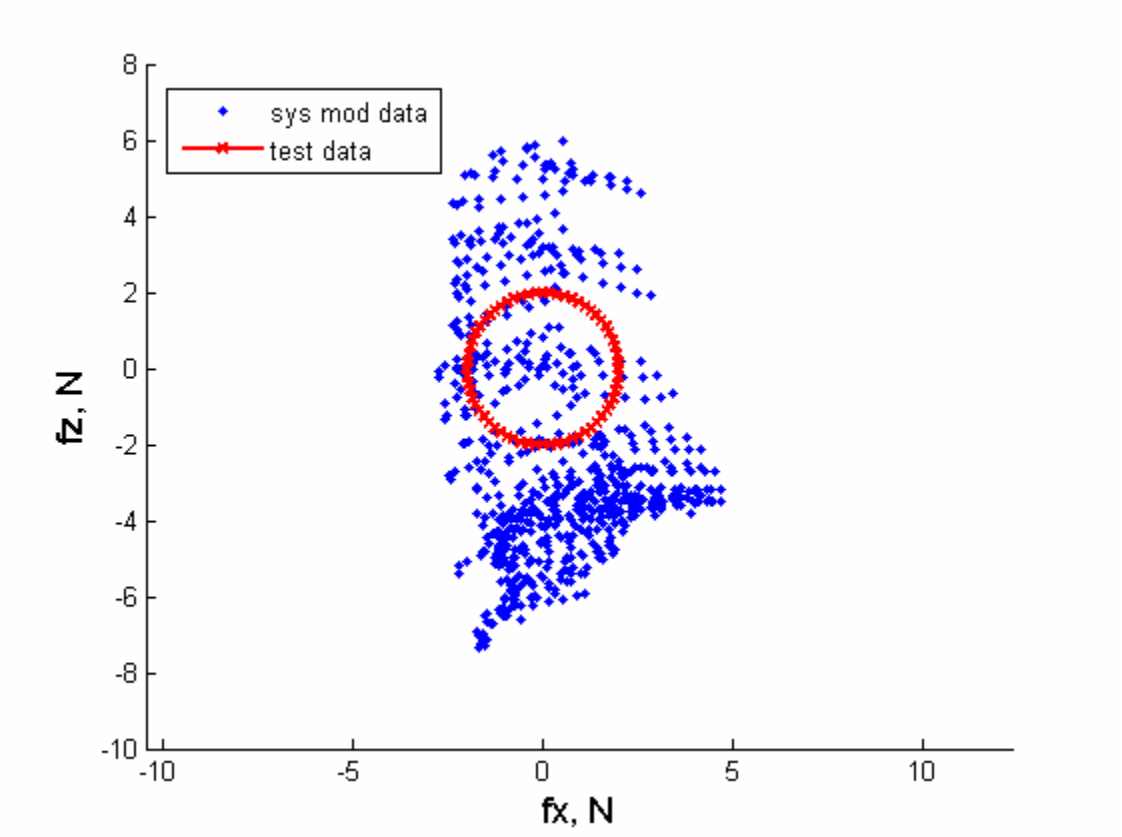


**Figure 21. Test forces used to plot the energy circles in Figure 20.**

## Controller Testing

The inverse controller was trained on this unique solution. Forty test force vectors were randomly selected from within the training data range (Figure 22) for each experiment and the trained inverse controller predicted the pulsewidths for these. Forty test force pairs generally allowed us to span the force range while maintaining stimulation time relatively short and within experimental time constraints.

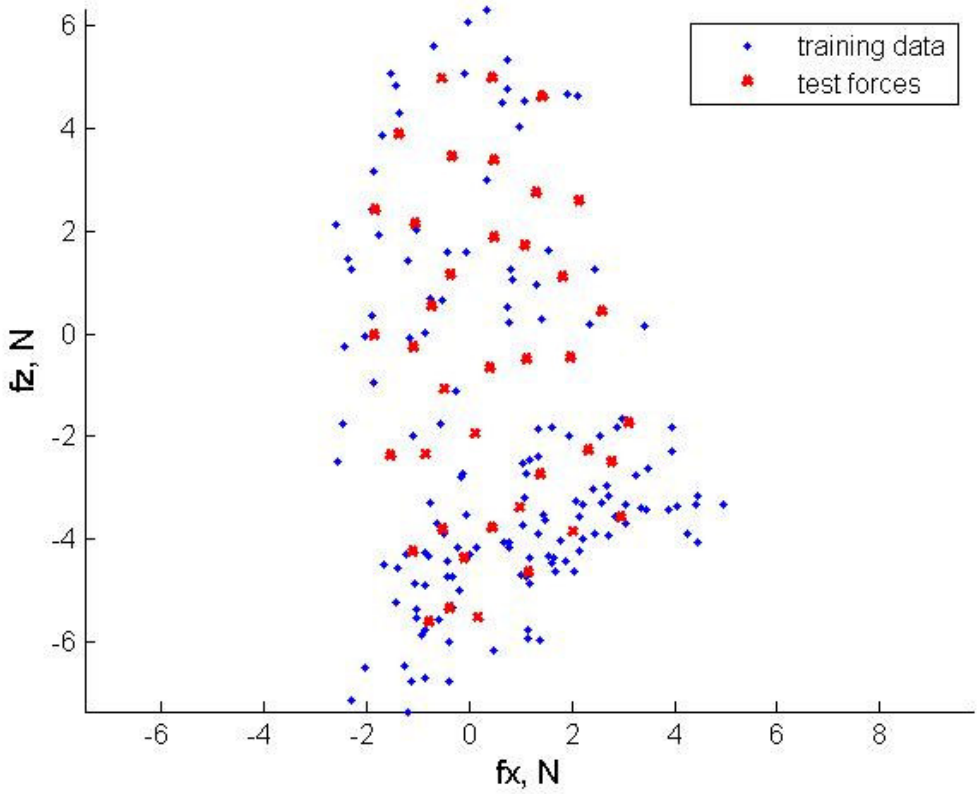


**Figure 22. Test forces (experiment 7) superimposed on the training force space for the system model. The test target forces were randomly selected to span the majority of the force range.**

The muscles were stimulated for two seconds with each of the predicted pulsewidth combinations, followed by ten seconds of rest. The muscles were stimulated using the predicted pulsewidths at two different times to measure system variability. The resulting thumb-tip forces were measured during muscle stimulation. The sequential target and actual test forces are shown in Figure 23. For most experiments, there was a bias on the z axis with good force matching on the x axis, but others had a scale difference in addition to the bias.

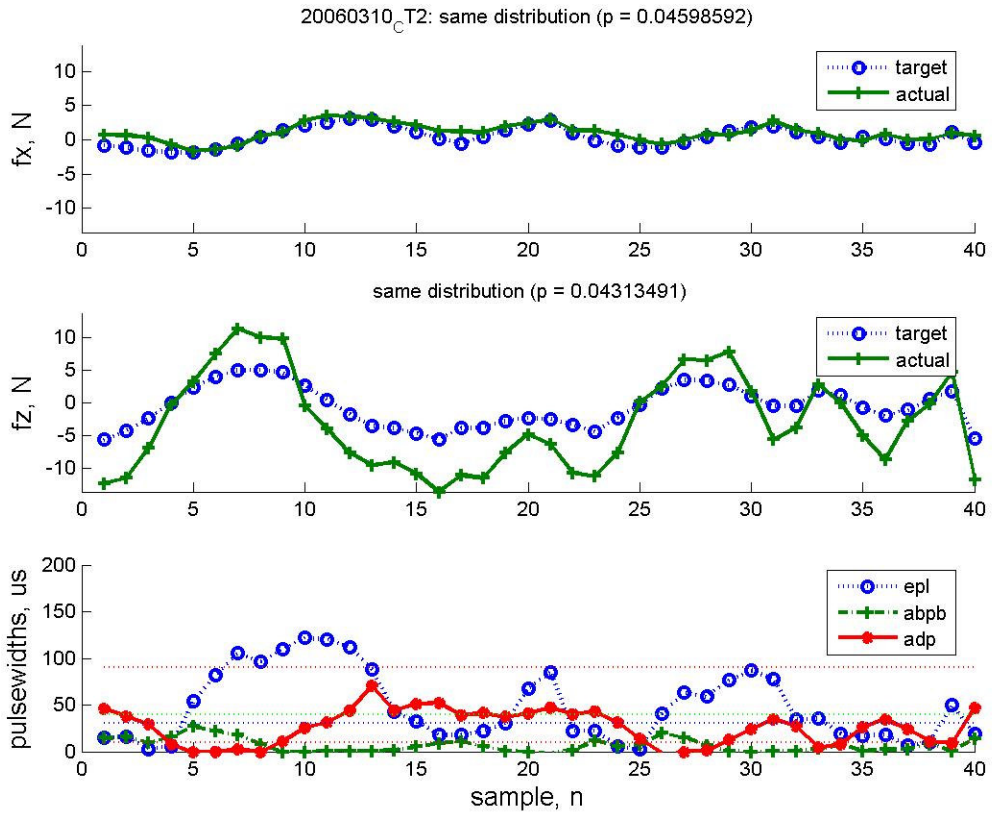


**Figure 23. Sequential target and actual test forces and predicted pulsewidths for experiment 7. The target and actual forces seem to have systematic errors.**

We performed a statistical analysis to investigate whether the actual forces matched the targets (i.e., their differences were due to limb model variability and not controller errors). We first determined system variability $S_1^2$ (1), which indicates how much the end-point forces vary with time, by stimulating the muscles at two different times using the pulsewidths predicted by the controller and measuring the corresponding forces ($F_{actual1}$ and $F_{actual2}$).

$$S_1^2 = system\_variability = \frac{\sum_{i=1}^{k}\left(F_{actual1}(x_i) - F_{actual2}(x_i)\right)^2}{k} \qquad (1)$$

The system variability was then compared to the target force variance. We considered the system as controllable if system variability was less than 30% of the variance of the target forces (i.e., $S_1^2 < 0.3\sigma_{target}^2$).

We assessed controller performance by comparing total variability $S_2^2$ (2) and system variability using a Modified Levene test with $F_o = S_1^2 / S_2^2$ for equality of variances ($H_o : S_1^2 = S_2^2$).

$$S_2^2 = total\_variability = \frac{\sum_{i=1}^{k}\left(F_{target}(i) - F_{actual1}(x_i)\right)^2}{k}$$ , where $x_i$ is the pulsewidths vector at iteration $i$ and $k$ is the number of input/output combinations in the data set. (2)

We rejected the null hypothesis ($H_o$) when $F_o > F_{\alpha/2, k_1-1, k_2-1}$ or $F_o < F_{1-(\alpha/2), k_1-1, k_2-1}$. $F_{\alpha/2, k_1-1, k_2-1}$ and $F_{1-(\alpha/2), k_1-1, k_2-1}$ are the upper .025 and lower 0.975 ($\alpha$=0.05) percentage points of an F distribution with $k_1$-1 and $k_2$-1 degrees of freedom. Controllers were considered successful when the null hypothesis was valid for both axes.

Target and actual forces matched with p-values > 0.3 in seven of the nine experiments (78%) conducted to date, but only for the x axis. Target and actual forces did not match along both axes for any experiment. However, the data distributions suggested their differences might be the result of systematic errors in the form of biases and/or scale differences (Figure 23).

While random errors could result in an inefficient controller, systematic errors (e.g., bias error) could, in theory, be corrected or compensated for.

We estimated the bias error between the average target forces ($\overline{F}_{target}$) and the average actual forces ($\overline{F}_{actual}$).

$$bias\_error = \overline{F}_{target} - \overline{F}_{actual}$$ , where $\overline{F} = \frac{\sum_{i=1}^{k} F_i}{k}$ (3)

We removed the bias error (Figure 24) and calculated the variability between the target ($F_{target}$) and the new actual forces ($F_{actual1}$), i.e., residual variability $S_3^2$ (4).

$$S_3^2 = residual\_variability = \frac{\sum_{i=1}^{k}\left(F_{target}(i) - F_{actual1}(x_i) - bias\right)^2}{k}$$ (4)

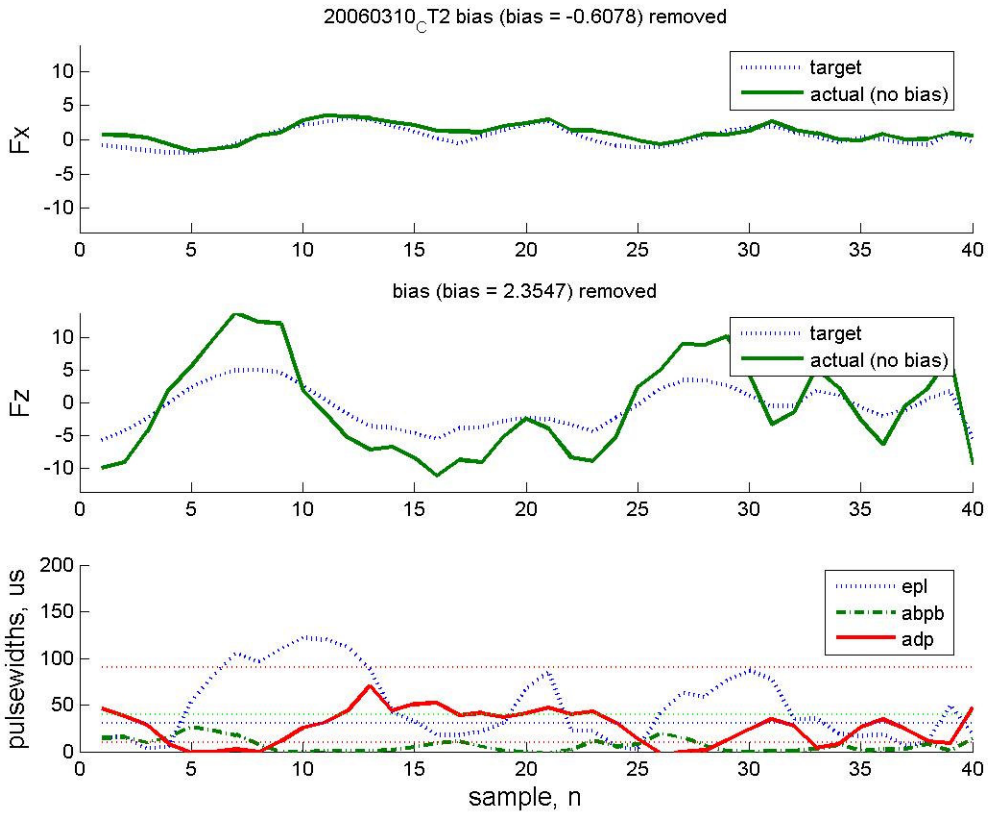


**Figure 24. Sequential target and actual test forces, as well as predicted pulsewidths (experiment 7). Bias has been removed from the actual forces.**

We compared the residual variability ( $S_3^2$ ) to the system variability by testing a second hypothesis $H_{o\_b} : S_3^2 = S_1^2$, with the same rejection criteria as above, to determine if the target and actual forces matched after removal of the bias.

The target and actual forces matched for five out of nine experiments (67%) on both axes with p > 0.08 after removal of the bias.

For the four experiments where the second hypothesis was rejected, we investigated scale errors as another possible source of systematic errors. We calculated the correlation between the target and actual forces.

Three out of these four experiments (75%) had a correlation coefficient > 0.89, indicating a very strong correlation between the target and actual forces (Figure 25), even in the presence of small random errors (Figure 26).

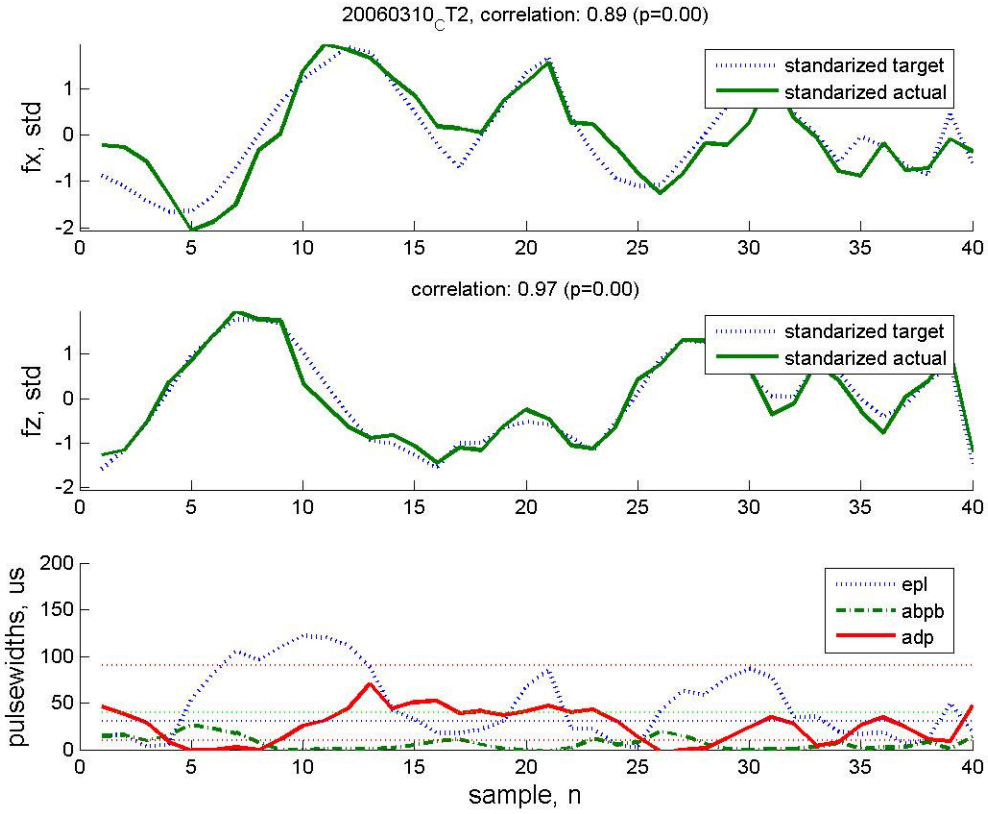


**Figure 25. Correlation between target and actual forces.**

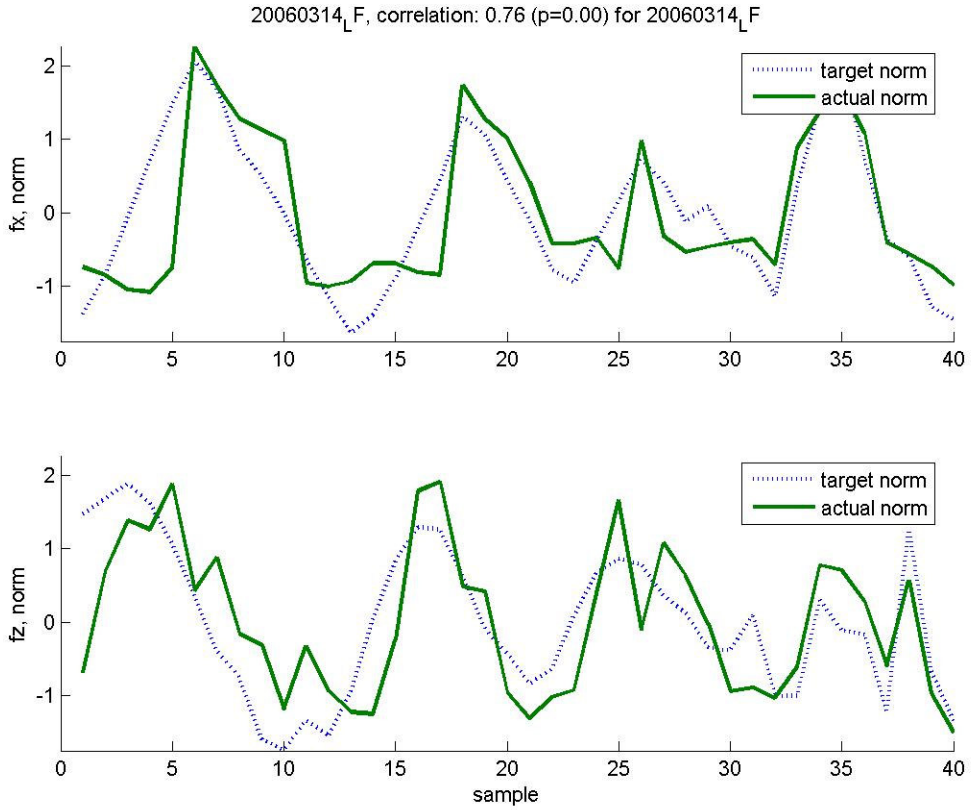


**Figure 26. Target and actual test forces for experiment 8. The random errors are not large enough to prevent good force tracking. The bias has been removed and the correlation estimated.**

Controllers were deemed successful when we failed to reject *Ho*, *Ho_b*, or when the correlation coefficient was larger than 0.6. If the first hypothesis could not be rejected, the total variability was explained by the system variability. When the second hypothesis was not rejected, the total variability was increased by a bias-inducing factor that could be compensated for. If both hypothesis were rejected but the correlation coefficients were larger than 0.6, the total variability was affected by a scaling factor that could possibly be compensated for, although the important fact is that force modulation was obtained.

## Conclusions

Experiments in seven human subjects testing control of two-degree-of-freedom force vectors at the thumb tip by stimulating three muscles showed that it is possible to design an inverse controller from input-output data.

We also showed that we can use a system model to eliminate time-variance from the raw data and an optimization process to the redundancy problem by reducing coactivation.

Some errors were present but significant correlations between the target and actual forces demonstrate the ability of the inverse controller to coordinate multiple interacting muscles without having a mechanistic model of the limb (i.e., the inverse controller can predict the inputs required to achieve target outputs within the training data space)

**Next Quarter**

We will investigate the sources for the systematic errors and will test the controller isometrically with spinal cord injured human subjects.

**References**

Kilgore K.L. (1987) "Force vector recruitment of electrically stimulated paralyzed thenar muscles with application to functional neuromuscular stimulation", M.S. Thesis, Case Western Reserve University.

Kirsch RF. et al, (2005) "Restoration of Hand and Arm Function by Functional Neuromuscular Stimulation", Quarterly Progress Report #18, NIH Neuroprosthesis Contract N01-NS-1-2333, October.

Lujan J.L., Crago P.E. (2004) "Computer-based test-bed for clinical assessment of hand/wrist feed-forward neuroprosthetic controllers using artificial neural networks", Med Biol Eng Comput., 42(6), Nov, 754-61.